A practical metric for estimating the current climate forcing of natural mires

Janne Rinne[1], Juha-Pekka Tuovinen[2], Annalea Lohila[2,3]

1) Natural Resources Institute Finland, Helsinki, Finland
2) Finnish Meteorological Institute, Helsinki, Finland
3) INAR/Physics, University of Helsinki, Finland

This is a non-peer-reviewed preprint submitted to EarthArXiv.

The manuscript is currently under review in Environmental Research Letters, submitted on November 28, 2024, this revised version submitted on March 27, 2025.

Abstract: Commensuration of the radiative effects of different greenhouse gases (GHGs) is crucial for understanding the effects of land cover and ecosystem changes on the global climate. However, none of the current commensuration approaches are suitable for addressing the current climatic effect of mire ecosystems as compared to the situation in which such mires would not exist. The mire ecosystems have accumulated carbon for millennia, creating a negative perturbation to the atmospheric carbon dioxide content, but at the same time they emit methane into the atmosphere. Thus, the functioning of mires involves GHG fluxes with opposing effects on Earth's radiative balance. Here, based on a simple radiative forcing (RF) model, we propose a new metric for commensuration of the effects of accumulated carbon and methane emission (ACME) on Earth's energy balance. This ACME approach is applicable to natural mires with a significant part of their carbon accumulated more than 1000 years ago and requires relatively few input data. We demonstrate the feasibility of the ACME approach by applying it to a set of northern mires. The ACME-based RF estimate indicates that these mires have a cooling effect on the current climate, contrary to what a global warming potential-based calculation suggests, since the climatic effect is dominated by the sustained carbon accumulation. By applying the new metric with varying estimates of the total carbon storage and methane emission of northern mires, we estimate the current RF of these mires to range from –0.49 to –0.26 W m^{-2}.

1. Introduction

By sequestering atmospheric carbon dioxide (CO_2), mire ecosystems have accumulated vast amounts of carbon (C) over several millennia, thus naturally reducing the

atmospheric CO_2 content. For example, northern (>45°N) mires contain 250–400 Pg of C (Turunen et al., 2002). At the same time, these ecosystems act as significant sources of methane (CH_4) into the atmosphere, with current emission of 31–38 Tg(CH_4) yr^{-1} (Peltola et al., 2019). The ecosystem–atmosphere exchange of these two greenhouse gases (GHGs) has therefore created climate forcing components of opposing directions, CO_2 uptake cooling and CH_4 emission warming the global climate (e.g. Whiting and Chanton, 2001; Frolking et al., 2006).

The atmospheric concentration dynamics resulting from sustained surface fluxes follow very different trajectories for CO_2 and CH_4. For CH_4, with its atmospheric lifetime of about 10 years, a sustained emission will in a few decades create a steady state of a positive but constant concentration perturbation, where the sinks, mainly atmospheric oxidation by hydroxyl radical, are balancing the emission (Frolking et al., 2006). For CO_2, however, no steady state is established, and a sustained ecosystem sink generates an ever-increasing negative concentration perturbation (Frolking et al., 2006). This is due to the very long response times of some of the processes equilibrating a perturbance to the atmospheric CO_2 concentration (Joos et al., 2013). On the other hand, CH_4 has a higher radiative efficiency than CO_2, which means that a CH_4 molecule added to the atmosphere will induce a greater warming effect than an additional CO_2 molecule (Shine et al., 1990).

While the actual effect of GHGs on climate can be simulated with comprehensive, process-based Earth system models, various simplified approaches have been developed for comparing the climate effects of different GHGs (Fuglestvedt et al., 2003; Balcombe et al., 2018; Brandão et al., 2023). This can be accomplished via a metric that accounts for the different lifetimes and radiative efficiencies of GHGs, typically calculated with a parameterized radiative forcing (RF) model. These models can be used to dynamically calculate the RF due to GHG fluxes, negative or positive, of different ecosystems over a period ranging, for example, from a single forest rotation period (Lohila et al., 2010) to the whole Holocene (Mathijssen et al., 2014, 2017, 2022). In applications of this kind, the calculation of RF dynamics requires a reconstruction of the GHG flux history or a scenario for future fluxes.

The modelled RF can be processed into the global warming potential (GWP) that provides conversion to a unit of CO_2 equivalent (CO_2-eq), which is the most commonly used metric

for commensuration[1] of climatic effects of different GHGs (Shine et al., 1990; Fuglestvedt et al., 2003). The practical usage of GWPs avoids an explicit calculation of RF, as GWP represents a constant equivalence factor between a non-CO_2 GHG and CO_2. This coefficient is obtained by integrating the RF following a pulse emission of the GHG in question, typically over 20, 100 or 500 years, and relating this to the integrated RF of a similar mass pulse of CO_2 (Shine et al., 1990). The GWP approach is most appropriate for expressing anthropogenic emissions in commensurate units, in which case an annual emission, for example, can be well expressed as an individual, short-term pulse. However, GWPs continue to be used for the sustained GHG fluxes of natural ecosystems as well (e.g. Nykänen et al., 1995; Johansson et al., 2006; Rinne et al., 2007; Hugelius et al., 2023; Virkkala et al., 2024) despite the justified criticism against this (Frolking et al., 2006; Neubauer and Megonigal, 2015).

As an alternative to the GWP, Neubauer and Megonigal (2015, 2019) recommended the so-called sustained global warming potential (SGWP), originally called the step-change GWP (e.g. Johnson and Derwent, 1996), to be preferred if the GHG exchange should be considered a continuous process rather than a short-term event. Obviously, this is the case with natural ecosystems. Similarly to the GWP, the SGWP refers to a single number per GHG and time horizon. However, it is important to note that also any SGWP-based conversion to CO_2-eq implicitly or explicitly refers to a reference state, be it the GHG exchange before a land use or land cover change, or a nominal zero GHG exchange. Hence, such calculation corresponds to the climatic effect of a constant step change in GHG flux rather than that of an actual long-term GHG flux, whether constant or variable, as such. Similarly to the GWP-based approach, the SGWP has been used to answer questions for which it is not fully applicable for (e.g. Yuan et al., 2021; Virkkala et al., 2024). Another alternative to the GWP is its modification known as the GWP* (Allen et al., 2018; Lynch et al., 2020), in which the cumulative CO_2-eq exchange, calculated from CO_2 and CH_4 exchange with a 20-year time horizon, is used to quantify the climatic effect of the changes in these GHG fluxes. However, this approach requires data or assumptions on the temporal trajectories of the exchange of these GHGs.

[1] Commensuration is defined as the comparison of different entities according to a common metric (Espeland and Stevens, 1998).

In conclusion, neither the GWP- nor the SGWP-based conversion to CO_2-eq adequately represents the actual flux dynamics and related climate forcing in the case of sustained GHG exchange of natural ecosystems. On the other hand, the use of GWP* requires long-term trajectories for GHG fluxes, which are not often readily available, and explicit calculation of RF additionally depends on modelling resources. Hence, our aim here is to present a simple metric for quantifying the current climatic effect that can be justifiably attributed to the past and present GHG exchange of natural mire ecosystems. Our approach is based on the important notion that these ecosystems have accumulated carbon for millennia, which should be accounted for when assessing their climatic effects. It has been suggested that the current RF of natural mires depends mainly on the accumulated C storage and the current CH_4 emission rate and thus could be quantified with these parameters with some information on peat initiation date (Frolking et al., 2006; Mathijssen et al., 2022). As some cryoturbated permafrost peatlands have been observed to emit nitrous oxide (N_2O, Repo et al., 2009) we supplement the new metric with this GHG for completeness' sake.

2. Radiative forcing due to atmospheric GHG perturbations

The radiative forcing due to a perturbation to the atmospheric mixing ratio of a well-mixed GHG, denoted by χ, can be expressed as

$$\Delta RF_\chi = \varepsilon_\chi \Delta c_\chi, \quad (1)$$

where ε_χ is the radiative efficiency and Δc_χ the mixing ratio change of χ (Shine et al., 1990). Assuming perfect mixing, c_χ is related to the atmospheric mass of χ, m_χ, by $c_\chi = \left(M_\mathrm{a}/\mu M_\chi\right) m_\chi$, where M_a is the mean molar mass of air, μ is the total mass of the atmosphere and M_χ is the molar mass of χ. We derived the radiative efficiencies from the RF parameterization of Meinshausen et al. (2020) as $\varepsilon_\chi = \partial RF_\chi / \partial c_\chi$ at a fixed reference c_χ of 420 ppm, 1920 ppb and 340 ppb for $\chi = CO_2$, CH_4 and N_2O, respectively. For details, see Supplement I.

The dynamics of m_χ associated with the mass flux F_χ to the atmosphere can be modelled as

$$m_\chi(t) = m_\chi(0) R_\chi(t) + \int_0^t F_\chi(s) R_\chi(t-s) ds, \ t > 0, \quad (2)$$

where t is time and R_χ the atmospheric impulse–response function of χ (Oeschger and Heimann, 1983; Enting, 2007). The impulse-response functions of GHGs can be described by a series of exponential functions. For CH_4 and N_2O, we adopted first-order decay with atmospheric lifetimes of $\tau_{CH4} = 11.8$ yr and $\tau_{N2O} = 109$ yr (Forster et al., 2021). For CO_2, the dynamics are more complex as there are processes acting in widely differing time scales. Thus, we modelled the atmospheric CO_2 mass, m_{CO2}, affected by the net atmosphere–ecosystem CO_2 flux F_{CO2}, with the following impulse–response formulation:

$$m_{CO2,i}(t) = m_{CO2,i}(0)e^{-t/\tau_{CO2,i}} + \int_0^t \alpha_i F_{CO2}(s)e^{-(t-s)/\tau_{CO2,i}}ds,\ i = 0, \dots, n, \quad (3)$$

$$m_{CO2}(t) = \sum_{i=0}^{n} m_{CO2,i}(t), \quad (4)$$

which shows that the total CO_2 mass is divided into $n + 1$ compartments, each carrying a mass of $m_{CO2,i}$. One of these compartments has a very long perturbation time scale ($\tau_{CO2,0} = \infty$), thus resulting in a permanent change, while in the others an atmospheric mass pulse decays with a characteristic, finite time scale ($\tau_{CO2,i}, i = 1, \dots, n$). The CO_2 flux is divided into these conceptual reservoirs according to the fractions α_i. Here, $n = 3$, and we parameterized the model according to Joos et al. (2013); for further details, see Supplement I.

Equation (2) can be numerically integrated in time, starting from an arbitrary initial mass and assuming any temporal flux trajectory. Figure 1 shows examples for hypothetical flux trajectories, for which it was assumed that F_{CO2} corresponds to the carbon accumulation rate (CAR) of the mire and $F_{CH4} = 0.2 \times$ CAR in terms of C (e.g. Rinne et al., 2018); for further examples, see Supplement II. The model results for these flux scenarios, extending well beyond the range of realistic cases, present a robust picture of the climate effect of the CO_2 exchange of a mire ecosystem: the perturbation to the current atmospheric CO_2 concentration depends mostly on the total amount of C accumulated during the history of the mire and is largely insensitive to any variations in the CAR trajectory followed more than about 1000 years ago. This shows that the radiative effect of the carbon exchange of a mire ecosystem can be estimated from its total carbon storage, as earlier suggested by Frolking et al. (2006) and Mathijssen et al. (2022).

In addition to numerical simulation, we showed analytically that, with a set of assumptions likely to be valid for many natural mire systems and consistent with the data availability in practice, the current RF due to the development and functioning of a mire

can be expressed to a close approximation by its total C storage and recent net fluxes of CO_2 and CH_4; see Supplement I for a full mathematical derivation. The specific CAR trajectory before about 1000 years ago has no significant effect on the current RF. Furthermore, this RF does not depend on the more recent CAR changes if these changes are modest. In the case of constant CAR in recent years, we can express the atmospheric perturbation to CO_2 mass simply as:

$$\Delta m_{CO2} \approx -\alpha_0 S_C + \beta F_{CO2}, \quad (5)$$

where S_C is the present areal mass density (kg m^{-2}) or the total mass (kg) of accumulated C, or C storage, in the ecosystem, and $\beta = \sum_{i=1}^{3} \alpha_i \tau_i \approx 99.9$ yr. Here, the βF_{CO2} term represents the transient contribution of C fluxes related to CAR during the last ~1000 yr; this term is generally small compared to the storage term (Supplement I).

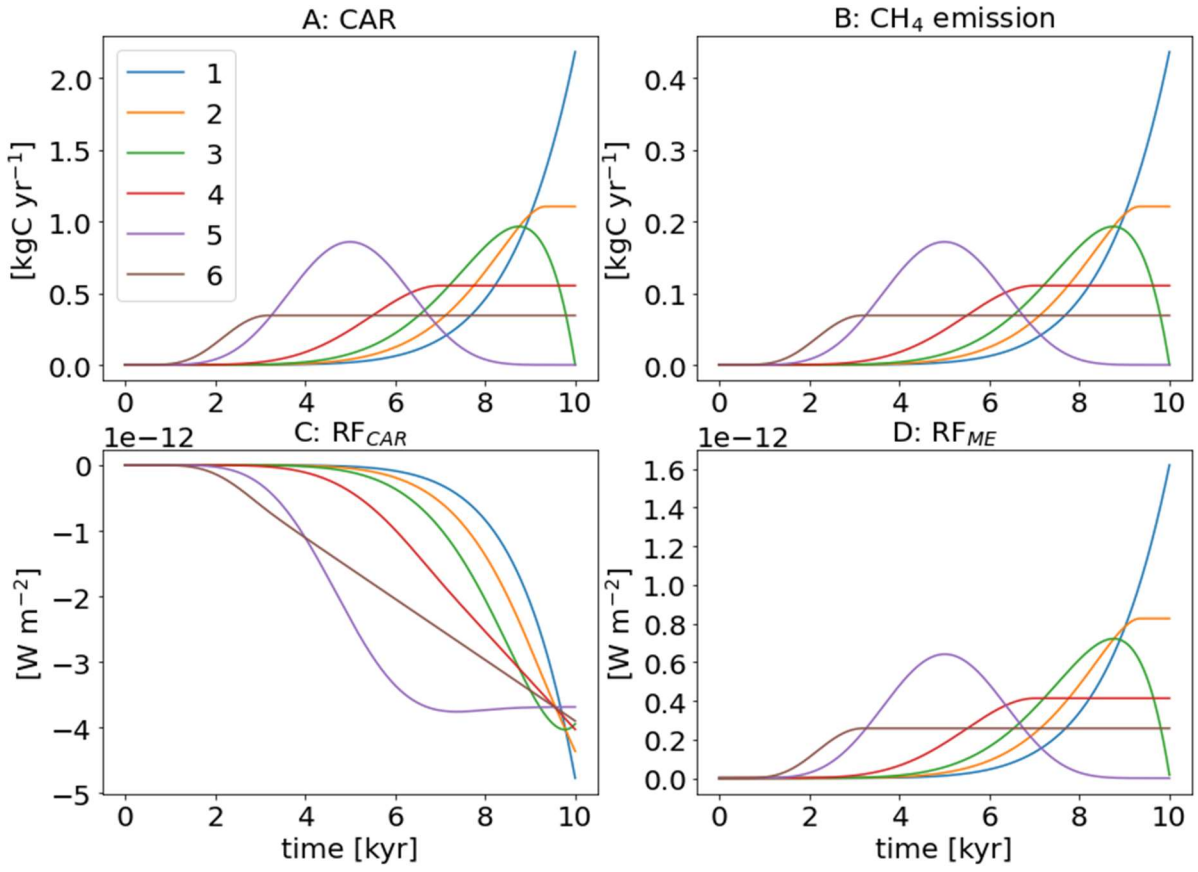

Figure 1: Radiative forcing created by C accumulation (mostly CO_2 exchange) and methane emission of a mire ecosystem. A: A selection of hypothetical CAR trajectories with the same total accumulated carbon over 10,000 years. B: CH_4 emission rates per assuming methane emission is 20% of CAR. C: RF caused by CAR. D: RF caused by CH_4

emission. Constant radiative efficiencies (Table SI.1) and perturbation time scales (Table SI.2) were assumed.

In contrast to CO_2, the RF due to the CH_4 emission of a mire is independent of the total CH_4 balance since peat initiation and only depends on the flux during the past few decades (Fig. 1). This is due to the short chemical lifetime of CH_4 in the atmosphere, which prevents a long-term or an accumulative concentration perturbation, as is the case with CO_2. The same applies to N_2O. Assuming constant CH_4 and N_2O flux for a period of multiple times their respective lifetimes, we obtain a steady-state atmospheric perturbation:

$$\Delta m_\chi = \tau_\chi F_\chi, \ \chi = \mathrm{CH_4}, \mathrm{N_2O}. \quad (6)$$

As long as peat accumulation has initiated at least 1000 years ago, the present-day RF is insensitive to the initiation date (Fig. 1). Even though the peat age does not directly affect the current RF, some data or assumptions on the age distribution of the peat layers are needed, as large recent changes in CAR can have a considerable transient effect on RF. These changes cannot be reduced to the total C storage but would need to be treated separately. Mostly, however, the differences in the current RF resulting from even recent CAR variations are relatively minor for any mire with a deep peat layer (Supplement I).

3. ACME approach for radiative forcing

Based on the rationale developed above, we conclude that the current climate impact of a mire ecosystem, expressed in terms of RF, can be justifiably approximated with data on the total C storage of the ecosystem and its CH_4 emission during the past 40 years. Thus, we propose a new climate metric, Accumulated Carbon – Methane Emission (ACME), which relates the C storage and CH_4 fluxes to the current RF via simple coefficients akin to GWP and SGWP (Eq. 7, Table 1). Also, N_2O emission and recent C exchange (the βF_{CO2} term in Eq. 5) can be included in ACME.

The radiative forcing of an ecosystem, according to the ACME approach, is defined as

$$RF_{\mathrm{ACME}} = -RFC_{\mathrm{S}} \times S_{\mathrm{C}} + RFC_{\mathrm{CH4}} \times F_{\mathrm{CH4}} + RFC_{\mathrm{CO2}} \times F_{\mathrm{CO2}} + RFC_{\mathrm{N2O}} \times F_{\mathrm{N2O}}, \quad (7)$$

where RFC_{S} and RFC_χ are the RF coefficients of C storage and GHG fluxes, respectively (Table 1). In most cases, it is sufficient to evaluate the two first terms in the right-hand side of Eq. (7), i.e., the terms that refer to the C storage and CH_4 emission. The two last

terms can be added into the calculation if there are data on recent CO_2 and N_2O fluxes. It is important to note that here F_{CO2} corresponds to the net change in the atmospheric CO_2 mass and thus equals CAR, i.e., the balance formed by the atmosphere–ecosystem fluxes of CO_2 and CH_4 and lateral C flow assuming that the C associated with CH_4 and lateral flow is oxidized to CO_2 and rapidly returned to the atmosphere.

Table 1. Radiative Forcing Coefficients (RFC) for conversion of the densities of ecosystem C storage and CH_4, CO_2 and N_2O fluxes to ACME radiative forcing.

	RFC
C storage	1.39×10^{-15} W m^{-2}/(kg C m^{-2})
CH_4 flux	2.27×10^{-12} W m^{-2}/(kg CH_4 m^{-2} yr^{-1})
Net CO_2 flux	1.74×10^{-13} W m^{-2}/(kg CO_2 m^{-2} yr^{-1})
N_2O flux	3.90×10^{-11} W m^{-2}/(kg N_2O m^{-2} yr^{-1})

The ACME approach can be used to estimate the climatic effect of a mire system with a minimal set of measurement data. The data needed for ACME include at least one peat core from the mire surface to the mineral soil for determination of the C storage density, and the annual CH_4 emission, for example measured by an eddy covariance (EC) system or a number of flux chambers (Bansal et al., 2023). Additionally, estimates of annual net C and N_2O fluxes can be introduced to elaborate the RF_{ACME} calculation. The flux data should represent the last 40, 1000 and 300 years for CH_4, CO_2 and N_2O, respectively.

4. Discussion

The appropriate method for quantification and commensuration of climatic effects of different GHGs crucially depends on the question to be addressed. The traditional GWP approach (Shine et al., 1990), in which the mass of a non-CO_2 GHG is simply converted to a unit of CO_2-eq, is suitable for answering the question on the relative climatic effects of different GHGs released in a pulse-like manner. Typically, anthropogenic emissions, where the baseline is "no emission", can be counted into this category. GWP can also be used for commensuration of short-duration changes in sustained GHG emissions, such as those due to temporary drought in wetland ecosystems (e.g. Rinne et al., 2020). In this particular case, the net flux expressed as CO_2-eq must be calculated from the difference

between the GHG exchange during the drought and a reference period. The SGWP approach, on the other hand, is suitable for commensuration of step-like change in sustained GHG emissions, such as those due to a land use change (Deshmukh et al., 2023). In this case, the CO_2-eq flux must be calculated from the difference in GHG exchange before and after the land use change.

Neither the GWP nor the SGWP approach relate the climatic effect to any specific time but average the effect over the given time horizon. For example, the climatic effect of a change in GHG exchange of a mire due to a drought year, as analyzed by the GWP approach, may indicate warming during the commonly used 100-year time horizon. However, this masks the actual RF dynamics with an initial cooling effect during the first decades after the drought and a warming effect thereafter (Rinne et al., 2020). The GWP coefficients also ignore the dependency of radiative efficiency on atmospheric GHG concentrations.

The ACME approach presented here has been designed to answer the question of what the current climatic forcing of an existing mire ecosystem is, compared to the situation that there was no ecosystem with significant C storage or CH_4 emission at the site, such as a tundra-like ecosystem. If the mire has developed replacing an earlier forest ecosystem on mineral soil, we should consider the difference in the C storage and CH_4 emission between these ecosystems. The C storage densities of boreal forest ecosystems on mineral soils (ca. 10 kg m^{-2}; Kauppi et al., 1997; Ilvesniemi and Liu, 2001; Liski et al., 2006) are typically very small compared to the C storage densities of many boreal mires (100–200 kg m^{-2}, See Table SIII.1). Furthermore, the CH_4 emission from such forest ecosystems is close to zero (Matson et al., 2009, Gillespie et al., 2024). Thus, even in this case, the ACME approach can provide a reasonable first approximation of the current climatic effect of the mire ecosystem.

We need to acknowledge some practical challenges in using the ACME metric. First, the CH_4 emission should be estimated for the past 30–40 years, while the longest measurement data series cover 10–20 years in length (e.g. Delwiche et al. 2021). Thus, we need to extrapolate these data back in time, making assumptions on the temporal representativeness of our data. This is an even more salient point for N_2O, which has a much longer atmospheric lifetime and typically shorter flux time series. Second, the available observations, both peat cores for C storage and flux chamber or EC

measurements for CH_4 emission, may not be spatially representative of the whole mire complex. This can be especially important in mires with a significant lateral expansion in recent times. Also, deriving CAR from peat core-based C accumulation may result in overestimation of the recent CAR (Young et al., 2019).

The lateral expansion of mire ecosystems may complicate the derivation of CAR (e.g. Mathijssen et al., 2022) and thus also the current RF of the whole mire. However, we can apply the ACME metric as a simpler "bucket view" that includes only the vertical peat growth, with the GHG exchange and C storage expressed per unit area, as indicated in Table 1. A more comprehensive "whole mire view", which in principle is equally applicable with Eq. (7), would include considerations of the lateral peat expansion and requires the C balance of the total mire area as input.

Commonly, GHG exchange measurements are conducted within the central area of a mire system, with peat depth and C storage also reported for this area. This is the case especially for EC measurements due to their requirement of large horizontally homogenous surface around the measurement tower. Thus, EC measurements may not represent the full mire area ignoring the spatial flux variability especially in the vicinity of the mire's edges. In the same vein, the C storage reported with EC measurements usually only represents the flux footprint. We can visualize this limited focus as a bucket of peat in the middle of peatland; this bucket represents a specific area (square metre, hectare, etc.) within the flux footprint and has a height of the average peat depth within this area. In this bucket, GHG exchange and C storage are laterally uniform, only the vertical growth of peat is considered. Thus, the accumulated C storage density can be obtained from even a single peat core extending from surface to the mineral soil below the peat layer.

The lateral growth of mire ecosystems can be an important determinant of their recent CAR and thus of their transient climatic effect. The variations of total CAR of mires depend strongly on the topography of the underlying soil, determining the lateral growth rate (Juselius-Rajamäki et al., 2023). In some mires, lateral growth has increased the total CAR approximately linearly while in others the total CAR has accelerated over time (Mathijssen et al., 2022). A higher (constant) CAR in recent times can be incorporated into the F_{CO2} term of Eq. (7), which in principle can be extended by assuming a

mathematically feasible lateral growth trajectory; a solution for linear growth of CAR is provided in Supplement I.

With the caveats discussed above, we can use the ACME approach to estimate the climatic effect of mires both for individual ecosystems and as aggregated regionally. For an illustrative example, we used the EC measurement data from five northern mires (Supplement III, Aurela et al., 2015, 2022, Heiskanen et al., 2023, Juutinen et al., 2013, Larsson et al., 2016, Mathijssen et al., 2022, Nilsson et al., 2008, Piilo et al., 2020, Rinne et al., 2018, Roulet et al., 2007; Yu et al., 2002) to calculate their climatic effect using the ACME approach (Fig. 2). For comparison, we also show the GHG fluxes expressed as CO_2-eq and the RFs corresponding to this GWP-based conversion. The ACME approach results in negative, i.e. cooling, RF for all the mires, as the effect of long-term C accumulation outweighs the warming effect of the present-day CH_4 emission. In contrast, the GWP approach leads to positive RF, i.e. a warming effect, at almost all sites; this illogicality results from the omission of the RF of sustained C sequestration from the atmosphere. The SGWP approach would suggest an even stronger warming effect as the SGWP coefficient of CH_4 is higher than the GWP of CH_4 (Neubauer and Megonigal, 2019). Furthermore, there is no statistically significant correlation between the GWP-based results and those of the ACME approach (Fig. 2). It is noteworthy how the (S)GWP-based results differ in a qualitative manner from those of the ACME approach.

To demonstrate the robustness of the ACME approach, we calculated RF dynamically using the explicit RF model for Mer Bleue, for which there is high-time-resolution CAR data available from the past 1000 years. The details of the computation are presented in Supplement III. Despite the relatively large changes in CAR within the last 500 years at Mer Bleue, the RF resulting from the ACME coefficients (-2.31×10^{-13} W m^{-2}) was very close to that obtained from the full impulse-response model (-2.35×10^{-13} W m^{-2}), which lends confidence to the ACME approach (Fig. SIII.1).

Furthermore, adopting the estimate of 250–400 Pg C for the C storage in mires north of 45 °N (Turunen et al., 2002) and the estimate of 31–38 Tg CH_4 yr^{-1} for CH_4 emission from these ecosystems (Peltola et al. 2019), we obtain an estimate of –0.49 to –0.26 W m^{-2} for the current RF due to the GHG dynamics of these mires. This is very similar to the range of -0.56 to -0.22 W m^{-2} estimated by Frolking and Roulet (2007) for the RF caused by the

northern mires. The similarity between the RF estimates arises from the similarities in the methods employed. However, while the modelling of Frolking and Roulet (2007) employed the CAR and methane trajectories over the Holocene, the ACME approach requires only data on the total accumulated carbon and recent methane emission. Both approaches suggest that the formation of northern mires during the Holocene has created a considerable cooling effect compared to a situation without their GHG exchange.

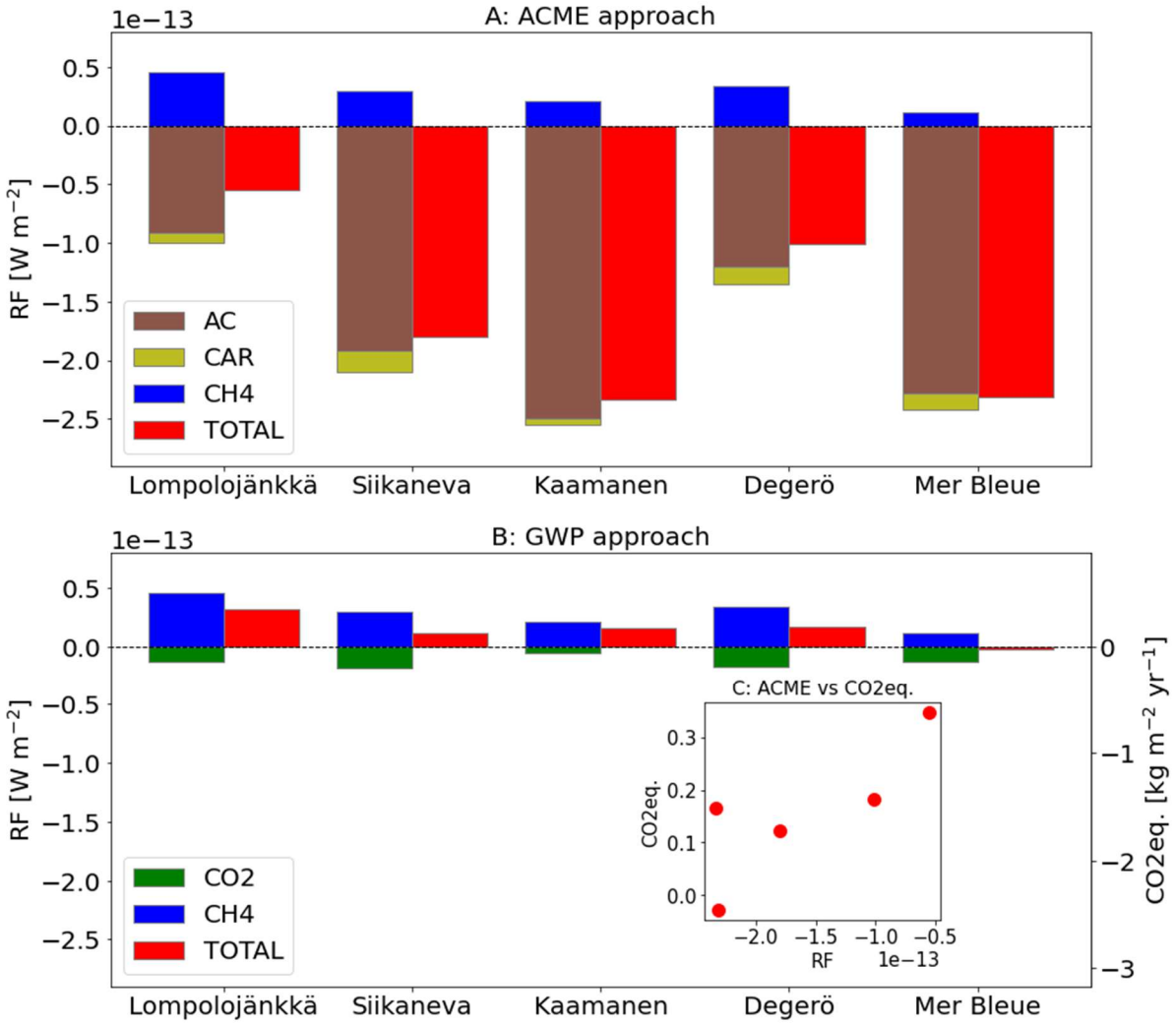

Figure 2. Radiative forcing of five northern mires, per m² of mire, calculated with the ACME (A) and GWP approaches (B). The ACME-based RF is calculated by Eq. (7) using data on accumulated C (AC), current C accumulation rate (CAR) and CH_4 flux (CH4) densities. The CAR is calculated as a difference between CO_2-C uptake, and the sum of CH_4-C emission and lateral C flux. The RF corresponding to the 100-year GWP is calculated using data on the current CO_2 flux (CO2) and CH_4 flux (CH4) densities as detailed in Supplement III. The insert C shows the relationship between the ACME-based

RF and the GWP-based CO_2-eq flux (Pearson's correlation r=0.81, two tailed p=0.097). The data used in calculation are presented in Table SIII.1.

As already discussed above, other metrics are more suitable for commensuration of the changes in GHG exchange caused by recent or planned land use changes. Especially useful approaches for this would be the explicit modelling of RF, and GWP*- or SGWP-based calculations. Finally, it should be noted that preservation of mires and other wetland ecosystems, their restoration, or construction of new wetlands may serve other purposes than climate change mitigation, such as biodiversity protection, flood risk and eutrophication mitigation and recreative purposes. Thus, the cost-benefit analysis of these actions cannot be based solely on their climatic effects.

5. Concluding remarks

We propose here a new ACME metric to estimate the current climatic effect of mire ecosystems, based on their accumulated carbon storage and recent methane emission rate. The metric is suitable for natural mires with a large carbon storage established more than 1000 years ago and requires only peat core data on accumulated carbon and measurements on annual methane emissions. The ACME metric indicates a considerable contemporary cooling effect by the northern mires formed during the Holocene, both for a selection of individual mires and globally. For estimation of the current climatic effect of mire systems, it would be beneficial that research reports, data publications and data repositories on carbon accumulation and GHG exchange of ecosystems, such as the FLUXNET products and ICOS Carbon Portal (Delwiche et al., 2021; Heiskanen et al., 2022), would include also the total carbon storage densities from the peat cores collected.

Acknowledgements: This research has been partly supported by the "Greenhouse Gas Fluxes and Earth System Feedbacks" (GreenFeedBack) project (no. 101056921), and "Upgrading knowledge and solutions to fast-track wetland restoration across

Europe"(WetHorizon) project (no. 101056848) from the European Union's Horizon Europe Framework Programme for Research and Innovation; by the "Peatland restoration for greenhouse gas emission reduction and carbon sequestration in the Baltic Sea region" (EU LIFE+ LIFE21-CCM-LV-LIFE PeatCarbon, no. 101074396) funded by the European Union; and by European Commission Just Transition Fund, through Council of Oulu Region (2021/900302/09).

References

Allen M R, et al. 2018 A solution to the misrepresentations of CO2-equivalent emissions of short-lived climate pollutants under ambitious mitigation. npj Clim Atmos Sci 1, 16.

Aurela M, Laurila T and Tuovinen J-P 2002 Annual CO2 balance of a subarctic fen in northern Europe: Importance of the wintertime efflux. *Journal of Geophysical Research* **107** 4607

Aurela M, Lohila A, Tuovinen J-P, Hatakka J, Penttilä T and Laurila T 2015 Carbon dioxide and energy flux measurements in four northern-boreal ecosystems at Pallas. *Boreal Environmental Research* **20** 455-473

Balcombe P, Speirs J F, Brandon N P and Hawkes A D 2018 Methane emissions: choosing the right climate metric and time horizon. *Environ. Sci.: Processes Impacts* **20** 1323-1339

Bansal S, Creed I F, Tangen B. A. *et al.* 2023 Practical Guide to Measuring Wetland Carbon Pools and Fluxes. *Wetlands* **43** 105, doi.org/10.1007/s13157-023-01722-2

Brandão M, Kirschbaum M U F and Cowie A L 2024 Evaluating metrics for quantifying the climate-change effects of land-based carbon fluxes. *Int J Life Cycle Assess* **29** 328–343 (doi: 10.1007/s11367-023-02251-0)

Delwiche et al. 2021 FLUXNET-CH4: a global, multi-ecosystem dataset and analysis of methane seasonality from freshwater wetlands. *Earth Syst. Sci. Data* **13** 3607–3689

Deshmukh C S *et al* 2023 Net greenhouse gas balance of fibre wood plantation on peat in Indonesia. *Nature* **616** 74-746 (doi: 10.1038/s41586-023-05860-9)

Enting I G 2003 Laplace transform analysis of the carbon cycle. *Environmental Modelling & Software* **22** 1488-1497 (doi: 10.1016/j.envsoft.2006.06.018)

Espeland W N and Stevens M L 1998 Commensuration as a Social Process. *Annual Review of Sociology* **24** 313-343

Forster P *et al* 2021 The Earth's Energy Budget, Climate Feedbacks, and Climate Sensitivity. In: Climate Change 2021: The Physical Science Basis. Contribution of Working Group I to the Sixth Assessment Report of the Intergovernmental Panel on Climate Change (ed. by V. Masson-Delmotte et al.), pp. 923–1054, Cambridge University Press, Cambridge, United Kingdom and New York, NY, USA, doi:10.1017/9781009157896.009.

Frolking S and Roulet N 2007 Holocene radiative forcing impact of northern peatland carbon accumulation and methane emissions. *Global Change Biology* **13** 1079-1088

Frolking S, Roulet N and Fuglestvedt J 2006 How northern peatlands influence the Earth's radiative budget: Sustained methane emission versus sustained carbon sequestration. *J Geophys Res* **111** G01008 (doi: 10.1029/2005JG000091)

Fuglestvedt J S, Berntsen T K, Godal O, Sausen R, Shine K P and Skodvin T 2003 Metrics of Climate Change: Assessing Radiative Forcing and Emission Indices. *Climatic Change* **58** 267–331 (doi: 10.1023/A:1023905326842)

Gillespie L M, Kolari P, Kulmala L, Leitner S M, Pihlatie M, Zechmeister-Boltenstern S and Díaz-Pinés E 2024 Drought effects on soil greenhouse gas fluxes in a boreal and a temperate forest. *Biogeochemistry* **167** 155–175

Heiskanen L, Tuovinen J-P, Vekuri V, Räsänen A, Virtanen T, Juutinen S, Lohila A, Mikola J and Aurela M 2023 Meteorological responses of carbon dioxide and methane fluxes in the terrestrial and aquatic ecosystems of a subarctic landscape. *Biogeosciences* **20** 545–572

Hugelius G, *et al* 2023 Two decades of permafrost region CO2, CH4, and N2O budgets suggest a small net greenhouse gas source to the atmosphere. *ESS Open Archive*. September 11, (doi: 10.22541/essoar.169444320.01914726/v1)

Ilvesniemi H and Liu C 2001 Biomass distribution in a young Scotts pine stand. *Boreal Environ. Res.* **6** 3-8.

Johansson T, Malmer N, Crill P M, Friborg T, Åkerman J H, Mastepanov M, Christensen T R 2006 Decadal vegetation changes in a northern peatland, greenhouse gas fluxes and net radiative forcing. *Global Change Biology* **12** 2352-2369

Joos F, et al 2013 Carbon dioxide and climate impulse response functions for the computation of greenhouse gas metrics: a multi-model analysis. *Atmospheric Chemistry and Physics* **13** 2793–2825

Johnson C E and Derwent R G 1996 Relative radiative forcing consequences of global emissions of hydrocarbons, carbon monoxide and NOx from human activities estimated with a zonally-averaged two-dimensional model. *Climatic Change* **34** 439–462

Juselius-Rajamäki T, Väliranta M and Korhola A 2023 The ongoing lateral expansion of peatlands in Finland. *Global Change Biology* **29** 7173–7191

Juutinen S, Väliranta M, Kuutti V, Laine A M, Virtanen T, Seppä H, Weckström J and Tuittila E-S 2013 Short-term and long-term carbon dynamics in a northernpeatland-stream-lake continuum: A catchment approach *J Geophys Res: Biogeosciences* **118** 171–183

Kauppi P E, Posch M, Hänninen P, Henttonen H M, Ihalainen A, Lappalainen E, Starr M and Tamminen P 1997 Carbon reservoirs in peatlands and forests in the boreal regions of Finland. *Silva Fennica* **31** 13-25.

Larsson A, Segerström U, Laudon H and Nilsson M B 2017 Holocene carbon and nitrogen accumulation rates in a boreal oligotrophic fen. *The Holocene* **27** 811-821 (doi: 10.1177/0959683616675936)

Liski J, Lehtonen A, Palosuo T, Peltoniemi M, Eggers T, Muukkonen A and Mäkipää R 2006 Carbon accumulation in Finland's forests 1922-2004 – an estimate obtained combination of forest inventory data with modelling of biomass, litter and soil. *Annals of Forest Science* **63** 687-697

Lohila A, Minkkinen K, Laine J, Savolainen I, Tuovinen JP, Korhonen L, Laurila T, Tietäväinen H and Laaksonen A 2010 Forestation of boreal peatlands: impacts of changing albedo and greenhouse gas fluxes on radiative forcing. *J. Geophys. Res. Biogeosci.* **115** 15 (doi: 10.1029/2010jg001327)

Lynch J, Cain M, Pierrehumbert R and Allen M 2020 Demonstrating GWP*: a means of reporting warming-equivalent emissions that captures the contrasting impacts of short- and long lived climate pollutants. *Environ. Res. Lett.* **15** 044023.

Mathijssen P J H, Tuovinen JP, Lohila A, Aurela M A, Juutinen S, Laurila T, Niemelä E, Tuittila ES and Väliranta M 2014 Development, carbon accumulation, and radiative forcing of a subarctic fen over the Holocene. *The Holocene* **24** 1156–1166 (doi: 10.1177/09596 83614 538072)

Mathijssen P J H, Kähkölä N, Tuovinen JP, Lohila A, Minkkinen K, Laurila T and Väliranta M 2017 Lateral expansion and carbon exchange of a boreal peatland in Finland resulting in 7000 years of positive radiative forcing, *J. Geophys. Res. Biogeosci.* **122** (doi: 10.1002/2016JG003749)

Mathijssen P J H., Tuovinen JP, Lohila A, Väliranta M and Tuittila ES 2022 Identifying main uncertainties in estimating past and present radiative forcing of peatlands. *Global Change Biology* **28** 4069-4084.

Matson A, Pennock D and Bedard-Haughn A 2009 Methane and nitrous oxide emissions from mature forest stands in the boreal forest, Saskatchewan, Canada. *Forest Ecology and Management* **258** 1073–1083

Meinshausen M *et al* 2020 The shared socio-economic pathway (SSP) greenhouse gas concentrations and their extensions to 2500. *Geoscientific Model Development* **13** 3571–3605 doi:10.5194/gmd-13-3571-2020.

Neubauer S C and Megonigal J P 2015 Moving Beyond Global Warming Potentials to Quantify the Climatic Role of Ecosystems. *Ecosystems* **18** 1000-1013 (doi: 10.1007/s10021-015-9879-4)

Neubauer S C and Megonigal J P 2019 Correction to: Moving Beyond Global Warming Potentials to Quantify the Climatic Role of Ecosystems. *Ecosystems* **22** 1931-1932 (doi: org/10.1007/s10021-019-00422-5)

Nilsson M, Sagerfors J, Buffam I, Laudon H, Eriksson T, Grelle A, Klemedtsson L, Weslien P and Lindroth A 2008 Contemporary carbon accumulation in a boreal oligotrophic

minerogenic mire – a significant sink after accounting for all C-fluxes. *Global Change Biology* **14** 2317-2332

Nykänen H, Alm J, Lång K, Silvola J and Martikainen P J 1995 Emissions of CH4, N2O and CO2 from a Virgin Fen and a Fen Drained for Grassland in Finland. *Journal of Biogeography* **22** 351-357

Oeschger H and Heimann M 1983 Uncertainties of predictions of future atmospheric CO2 concentrations. *J Geophys Res* **88** 1258-1262 (doi: 10.1029/JC088iC02p01258)

Peltola O et al 2019 Monthly Gridded Data Product of Northern Wetland Methane Emissions Based on Upscaling Eddy Covariance Observations. *Earth System Science Data* **11** 1263–1289

Piilo S et al 2020 Spatially varying peatland initiation, Holocene development, carbon accumulation patterns and radiative forcing within a subarctic fen. *Quaternary Science Reviews* **248** 106596 (doi: 10.1016/j.quascirev.2020.106596)

Repo M E, Susiluoto S, Lind S E, Jokinen S, Elsakov V, Biasi C, Virtanen T and Martikainen P J 2009 Large N2O emissions from cryoturbated peat soil in tundra. *Nature Geoscience* **2** 189-192 (doi: 10.1038/NGEO434)

Rinne J, Riutta T, Pihlatie M, Aurela M, Haapanala S, Tuovinen JP, Tuittila ES and Vesala T 2007 Annual cycle of methane emission from a boreal fen measured by the eddy covariance technique. *Tellus* **59B** 449-457

Rinne J *et al* 2018 Temporal variation of ecosystem scale methane emission from a boreal fen in relation to temperature, water table position, and carbon dioxide fluxes. *Global Biogeochemical Cycles* **32**, 1087-1106

Rinne J *et al* 2020 Effect of the 2018 European drought on methane and carbon dioxide exchange of northern mire ecosystems. *Philosophical Transactions of the Royal Society – B* **375** 20190517.

Roulet N T, Lafleur P M, Richard P J H, Moore T R, Humphreys E R and Bubier J 2007 Contemporary carbon balance and late Holocene carbon accumulation in a northern peatland. *Global Change Biology* **13** 397-411 (doi: 10.1111/j.1365-2486.2006.01292.x)

Shine K P, Derwent R G, Wuebbles D J and Morcrette JJ 1990 Radiative forcing of climate. In: Climate Change: The IPCC Scientific Assessment (Eds. J.T. Houghton, G.J. Jenkins & J.J. Ephraums), Cambridge University Press, Cambridge, UK.

Turunen J, Tomppo E, Tolonen K, and Reinikainen A 2002 Estimating carbon accumulation rates of undrained mires in Finland–application to boreal and subarctic regions. *The Holocene* **12** 69–80 (doi: 10.1191/0959683602hl522rp)

Virkkala AM *et al* 2024 High-resolution spatial patterns and drivers of terrestrial ecosystem carbon dioxide, methane, and nitrous oxide fluxes in the tundra. *Biogeosciences* **21** 335-355

Whiting G J and Chanton J P 2001 Greenhouse carbon balance of wetlands: methane emission versus carbon sequestration. *Tellus* **53B** 521–528

Young D M, Baird A J, Charman D J, Evans C D, Gallego-Sala A V, Gill P J, Hughes P D M, Morris P J and Swindles G T 2019 Misinterpreting carbon accumulation rates in records from near-surface peat. *Scientific Reports* **9** 17939 (doi: 10.1038/s41598-019-53879-8)

Yu, Z.C.; Bhatti, J.S.; Apps, M.J., technical coordinators. 2002. Long Term Dynamics and Contemporary Carbon Budget of Northern Peatlands. Proc. International Workshop on Carbon Dynamics of Forested Peatlands: Knowledge Gaps, Uncertainty, and Modeling Approaches, 23-24 March 2001, Edmonton, AB. Nat. Resour. Can., Can. For. Serv., North. For. Cent., Edmonton, AB. Inf. Rep. NOR-X-383.

Yuan Y, Sharp S J, Martina J P, Elgersma K J and Currie W S 2021 Sustained-flux global warming potential driven by nitrogen inflow and hydroperiod in a model of Great Lakes coastal wetlands. *Journal of Geophysical Research: Biogeosciences* **126** e2021JG006242 (doi: 10.1029/2021JG006242)

A practical metric for estimating the current climate forcing of natural mires

Janne Rinne[1], Juha-Pekka Tuovinen[2], Annalea Lohila[2,3]

1) Natural Resources Institute Finland, Helsinki, Finland
2) Finnish Meteorological Institute, Helsinki, Finland
3) INAR/Physics, University of Helsinki, Finland

Supplement I: Derivation of radiative forcing equations of ACME approach

Radiative forcing (RF) at time t due to exchange of long-lived greenhouse gases (GHGs) between the atmosphere and an ecosystem was calculated as

$$\Delta RF_\chi(t) = \varepsilon_\chi(t)\Delta c_\chi(t) \quad \text{(SI. 1)}$$

where ε_χ is radiative efficiency, Δc_χ is the mixing ratio change of the well-mixed GHG denoted by χ (here, $\chi = CO_2$, CH_4 or N_2O), and the concurrent change in other GHGs is ignored. Radiative efficiency was calculated as a marginal RF change with respect to mixing ratio change at a reference mixing ratio $c_{\chi,0}$,

$$\varepsilon_\chi = \left.\frac{\partial RF_{\mathrm{f},\chi}}{\partial c_\chi}\right|_{c_\chi = c_{\chi,0}} \quad \text{(SI. 2)}$$

where the RF functions $RF_{\mathrm{f},\chi}$were obtained from the parametrization of Etminan et al. (2016) as adjusted by Meinshausen et al. (2020). The temporal variation of ε_χ indicated in Eq. (SI.1) results from its dependency on the atmospheric mixing ratio of the perturbed GHG and the other GHGs that have spectral overlap effects (Etminan et al., 2016). The adopted $c_{\chi,0}$ and corresponding ε_χ values are shown in Table 1. The reference mixing ratios represent the global annual averages observed in the early 2020s (Lan et al., 2025a,b). The radiative efficiencies include tropospheric and surface adjustments (+5% for CO_2, −14% for CH_4, +7% for N_2O; Forster et al., 2021); ε_{CH4} also includes the contribution of an additional, indirect RF induced by atmospheric chemistry affecting tropospheric ozone and stratospheric water vapour, while ε_{N2O} includes the indirect RF via the effect on stratospheric ozone and methane lifetime (Forster et al., 2021). Assuming perfect mixing, c_χ was related to the atmospheric mass of χ, Δm_χ, as

$$\Delta c_\chi = \left(M_\mathrm{a}/\mu M_\chi\right)\Delta m_\chi \quad \text{(SI. 3)}$$

where $M_\mathrm{a} = 28.97$ g mol^{-1} is the mean molar mass of air, $\mu = 5.135 \times 10^{18}$ kg is the total mass of the atmosphere (Trenberth and Smith, 2005), and M_χ is the molar mass of χ.

Table SI.1. Reference mixing ratios $c_{\chi,0}$ and the radiative efficiencies $\varepsilon_{\mathrm{m},\chi} = \left(M_\mathrm{a}/\mu M_\chi\right)\varepsilon_\chi$ derived from the RF parameterization of Meinshausen et al. (2020).

Gas χ	$c_{\chi,0}$ (ppm)	$\varepsilon_{\mathrm{m},\chi}$ (W m^{-2} kg^{-1})

CO_2	420	1.74×10^{-15}
CH_4	1.92	1.93×10^{-13}
N_2O	0.34	3.57×10^{-13}

We modelled the mass balance of χ with an impulse–response function, which models the linear response to external perturbation (Oeschger and Heimann, 1983; Enting, 2007)

$$m_\chi(t) = m_\chi(0)R_\chi(t) + \int_0^t F_\chi(s)\, R_\chi(t-s)ds, \;\; t > 0 \tag{SI. 4}$$

where R_χ is the impulse–response function representing the dynamics of χ in the atmosphere, and F_χ is input to the system, here corresponding to carbon accumulation rate (CAR) resulting from the atmosphere–ecosystem exchange. For CO_2, we assumed that the mass flux F_{CO2} is divided into non-interacting conceptual reservoirs with characteristic adjustment or perturbation time scales. One of these reservoirs, with mass $m_{CO2,0}$, represents a cumulative effect corresponding to very slow geological responses to atmospheric perturbation, and the corresponding first-order time scale,$\tau_{CO2,0}$, is set to infinity; the CO_2 mass of the other reservoirs, $m_{CO2,i}$, $i = 1,\ldots,n$, decay with the finite first-order time scales of $\tau_{CO2,i}$, respectively, i.e., $R_{CO2,i}(t) = e^{-t/\tau_{CO2,i}}$. The contribution of the input flux to these reservoirs is expressed as fractions α_i with $\sum_{i=0}^{n}\alpha_i = 1$. Thus, the CO_2 mass balance dynamics for $t > 0$ can be written in a general form as

$$m_{CO2,0}(t) = m_{CO2,0}(0) + \int_0^t \alpha_0 F_{CO2}(s)\, ds \tag{SI. 5}$$

$$m_{CO2,i}(t) = m_{CO2,i}(0)e^{-t/\tau_{CO2,i}} + \int_0^t \alpha_i F_{CO2}(s)e^{-(t-s)/\tau_{CO2,i}}ds\,, \;\; i = 1,\ldots,n \tag{SI. 6}$$

$$m_{CO2} = \sum_{i=0}^{n} m_{CO2,i} \tag{SI. 7}$$

We adopted the widely used parametrization of Joos et al. (2013), in which $n = 3$ (Table 2).

Table SI.2. Parametrization of the atmospheric inpulse–response model (Joos et al., 2013).

i	0	1	2	3
α_i	0.2173	0.2240	0.2824	0.2763
$\tau_{CO2,i}$ (yr)	∞	394.4	36.54	4.304

In the present problem, we consider GHG exchange of an ecosystem starting at $t = 0$ (e.g., peat initialization time) and thus the appropriate initial condition for Eqs. (SI.5) and (SI.6) is $m_{CO2,i}(0) = 0$ (i.e., henceforth $\Delta m_\chi = m_\chi$). Thus, the solution of Eq. (SI.5) is

$$m_{\mathrm{CO2},0}(t) = \alpha_0 \int_0^t F_{\mathrm{CO2}}(s)ds \equiv -\alpha_0 S_{\mathrm{C}}(t) \quad \text{(SI. 8)}$$

i.e., $m_{\mathrm{CO2},0}(t)$ is proportional to the cumulative CAR, or the ecosystem carbon 'storage' $S_{\mathrm{C}}(t)$, irrespective of temporal flux variations. For $m_{\mathrm{CO2},i}$, $i = 1,2,3$, we first evaluate Eq. (SI.6) at a fixed time $t = t_{\mathrm{r}}$ to obtain

$$m_{\mathrm{CO2},i}(t_{\mathrm{r}}) = \alpha_i \int_0^{t_{\mathrm{r}}} F_{\mathrm{CO2}}(s) e^{-(t_{\mathrm{r}}-\mathrm{s})/\tau_{\mathrm{CO2},i}} ds \quad \text{(SI. 9)}$$

Taking this as a new initital state, we can write the solution for $t > t_{\mathrm{r}}$ as

$$m_{\mathrm{CO2},i}(t) = m_{\mathrm{CO2},i}(t_{\mathrm{r}}) e^{-(t-t_{\mathrm{r}})/\tau_{\mathrm{CO2},i}} + \alpha_i \int_{t_{\mathrm{r}}}^t F_{\mathrm{CO2}}(s) e^{-(t-s)/\tau_{\mathrm{CO2},i}} ds \quad \text{(SI. 10)}$$

This intermedite step was introduced to demonstrate explicitly that

$$m_{\mathrm{CO2},i}(t) \approx \alpha_i \int_{t_{\mathrm{r}}}^t F_{\mathrm{CO2}}(s) e^{-(t-s)/\tau_{\mathrm{CO2},i}} ds \quad \text{(SI. 11)}$$

if $t - t_{\mathrm{r}} \gg \max(\tau_{\mathrm{CO2},i})$, $i = 1,2,3$, because $e^{-(t-t_{\mathrm{r}})/\tau_{\mathrm{CO2},i}} \approx 0$, i.e., only the 'recent' ($t > t_{\mathrm{r}}$) fluxes significantly contribute to these terms of $m_{\mathrm{CO2}}(t)$.

Next, we consider some simplified CAR trajectories for $t > t_{\mathrm{r}}$, which may be possible to estimate from observations in practice and which do not necessitate numerical solution of the convolution integral (Eq. SI.11). First, we assume a constant CAR, $F_{\mathrm{CO2}}(t) = F, t > t_{\mathrm{r}}$. Based on the above derivation, the solution of Eqs. (SI.5)–(SI.7) with $m_{\mathrm{CO2},i}(0) = 0$ and $t > t_{\mathrm{r}}$ is

$$m_{\mathrm{CO2}}(t) = -\alpha_0 S_{\mathrm{C}}(t) + \sum_{i=1}^{3} m_{\mathrm{CO2},i}(t_{\mathrm{r}})\, e^{-(t-t_{\mathrm{r}})/\tau_{\mathrm{CO2},i}} + F \sum_{i=1}^{3} \alpha_i \tau_i \left(1 - e^{-(t-t_{\mathrm{r}})/\tau_{\mathrm{CO2},i}}\right) \quad \text{(SI. 12)}$$

where $m_{\mathrm{CO2},i}(t_{\mathrm{r}})$ depends on $F_{\mathrm{CO2}}(t)$ for $0 < t \leq t_{\mathrm{r}}$. If $t - t_{\mathrm{r}} \gg \max(\tau_{\mathrm{CO2},i})$, $i = 1,2,3$, then

$$m_{\mathrm{CO2}}(t) \approx -\alpha_0 S_{\mathrm{C}}(t) + F \sum_{i=1}^{3} \alpha_i \tau_i \equiv -\alpha_0 S_{\mathrm{C}}(t) + \beta F \quad \text{(SI. 13)}$$

where $\beta = \sum_{i=1}^{3} \alpha_i \tau_{\mathrm{CO2},i} \approx 99.85$ yr. The 'recent' time, $t > t_{\mathrm{r}}$, can be defined by requiring, for example, that $\sum_{i=1}^{3} \alpha_i \tau_i \left(1 - e^{-(t-t_{\mathrm{r}})/\tau_{\mathrm{CO2},i}}\right)/\beta > 0.95$, which equals $t - t_{\mathrm{r}} \gtrsim 1130$ yr $\left(\approx 3\tau_{\mathrm{CO2},1}\right)$.

If $F_{\mathrm{CO2}}(t) = F$ for $t > 0$, then $S_{\mathrm{C}}(t) = -Ft$, and we observe that $-\alpha_0 S_{\mathrm{C}}/m_{\mathrm{CO2}} > 95\%$ if $t \gtrsim 8700$ yr. Under such an assumption of constant CAR, the RF estimate based on $m_{\mathrm{CO2}}(t) \approx -\alpha_0 S_{\mathrm{C}}(t)$ provides a good approximation; this can be improved with data on the length of peat accumulation period as we can write $m_{\mathrm{CO2}}(t) \approx -(\alpha_0 + \beta/t) S_{\mathrm{C}}(t)$.

As another example, we assume that CAR is again arbitrary for $0 < t \leq t_{\mathrm{r}}$ and for $t > t_{\mathrm{r}}$ changes linearly with time, i.e., $F_{\mathrm{CO2}}(t) = \hat{F}_{\mathrm{r,CO2}} t + F_{\mathrm{r,CO2}}$, $t > t_{\mathrm{r}}$. Then the solution for $t - t_{\mathrm{r}} \gg \tau_{\mathrm{CO2},1}$ is

$$m_{\mathrm{CO2}}(t) \approx -\alpha_0 S_{\mathrm{C}}(t) + \left(\hat{F}_{\mathrm{r,CO2}} t + F_{\mathrm{r.CO2}}\right) \sum_{i=1}^{3} \alpha_i \tau_{\mathrm{CO2},i} - \hat{F}_{\mathrm{r,CO2}} \sum_{i=1}^{3} \alpha_i \tau_{\mathrm{CO2},i}^2 \quad \text{(SI. 14)}$$
$$\equiv -\alpha_0 S_{\mathrm{C}}(t) + \beta\left(\hat{F}_{\mathrm{r,CO2}} t + F_{\mathrm{r,CO2}}\right) - \gamma \hat{F}_{\mathrm{r,CO2}}$$

where $\gamma = \sum_{i=1}^{3} \alpha_i \tau_{\mathrm{CO2},i}^2 \approx 35230\ \mathrm{yr}^2$. To estimate the contribution of the storage term in this case, we assume that we can approximate the CAR trajectory by $F_{\mathrm{CO2}}(t) = \hat{F}t$ for $0 < t \leq t_{\mathrm{r}}$, and that the slope changes by a factor of k at $t = t_{\mathrm{r}}$, i.e., $F_{\mathrm{CO2}}(t) = k\hat{F}(t - t_{\mathrm{r}}) + \hat{F}t_{\mathrm{r}} = k\hat{F}t + (1-k)\hat{F}t_{\mathrm{r}}$ for $t > t_{\mathrm{r}}$. From this we obtain

$$m_{\mathrm{CO2}}(t) \approx -\alpha_0 S_{\mathrm{C}}(t) + [\beta(kt + (1-k)t_{\mathrm{r}}) - \gamma k]\hat{F} \quad \text{(SI. 15)}$$

where $S_{\mathrm{C}}(t)/\hat{F} = ½{t_{\mathrm{r}}}^2 + ½k(t^2 - t_{\mathrm{r}}^2) + (1-k)t_{\mathrm{r}}(t - t_{\mathrm{r}})$. The dependence of the storage term contribution on the slope multiplier and carbon accumulation period is shown in Figure SI.1. For example, $\alpha_0 S_{\mathrm{C}}/m_{\mathrm{CO2}} \approx 92\%$ at $t = 10{,}000$ yr if the slope of flux remains constant ($k = 1$). If $t = 10{,}000$ yr, $t - t_{\mathrm{r}} = 1000$ yr and $k \leq 5$, the error due to calculating the mass change from the carbon storage alone is less than 10%. Similar accuracy can be achieved for a shorter peat accumulation period if the acceleration in the recent CAR is modest. Overall, this analysis shows that the current atmospheric CO_2 mixing ratio change, and thus the related RF, can be approximated by the total carbon storage of a mire, and the estimate can be improved with data on the peat initialization date and recent changes in CAR.

It is important to note that the mass balance considerations above apply to the atmospheric GHG burden, and the CO_2 flux denoted by F_{CO2} does not equal the atmosphere–ecosystem flux. The carbon emitted by the ecosystem into the atmosphere as CH_4 originates from the CO_2 sequestered from the atmosphere and is predominantly oxidized back to CO_2, thus not contributing to Δm_{CO2} or ΔRF_{CO2}. In addition, the carbon storage of an ecosystem is affected by the lateral C flows, mainly in the form of dissolved organic carbon (DOC). This means that, when deriving the C storage S_{C} (Eq. SI.8) directly from the C content of the sampled peatland soil cores, it is assumed that all C removed from peat eventually returns to the atmospheric CO_2 pool. On the other hand, when measurement data on atmosphere–ecosystem fluxes are used as input for the atmospheric mass balance, F_{CO2} should be calculated as the sum of (typically opposite) CO_2 and CH_4 fluxes, preferably corrected for with data on DOC flux.

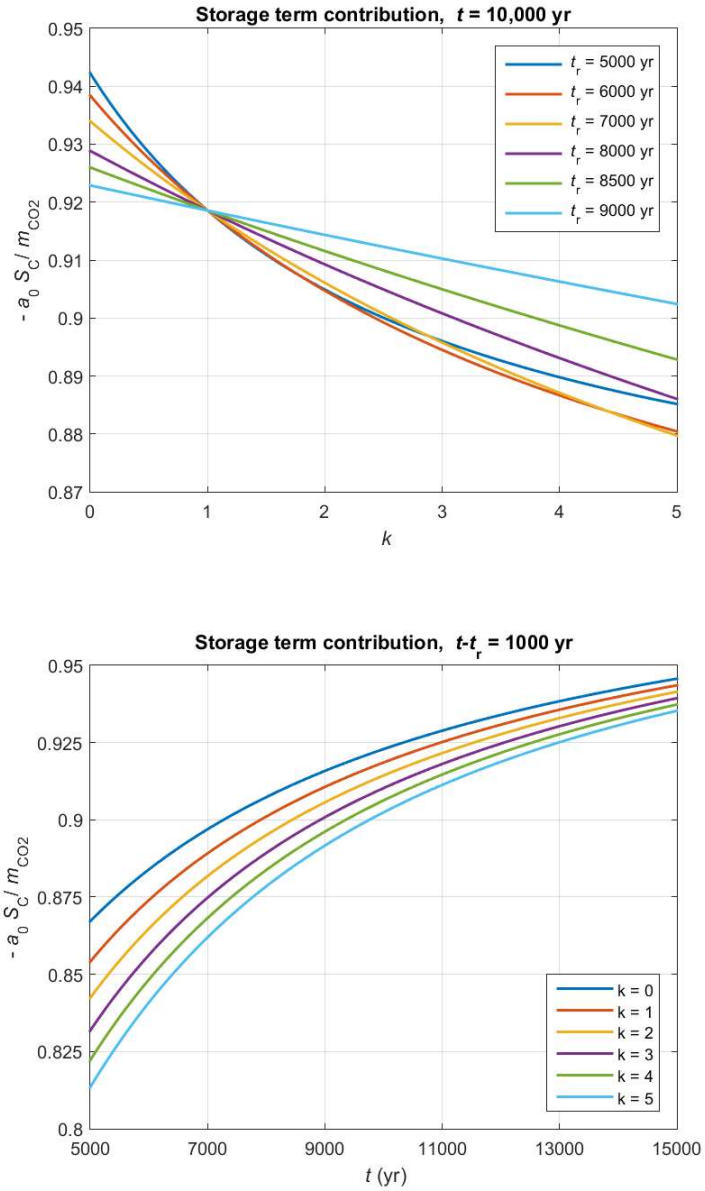

Figure SI.1. The contribution of the storage term to the modelled mass change as a function of multiplicative slope change in the assumed linear variation of CO_2 flux, with fixed $t = 10{,}000$ yr (top) and as a function of time, with fixed $t - t_r = 1000$ yr (bottom). The slope change occurs at $t = t_r$.

For CH_4 and N_2O, we assumed a first-order exponential impulse–response function, $R_\chi(t) = e^{-t/\tau_\chi}$, $\chi = CH_4, N_2O$, with $\tau_{CH4} = 11.8$ yr and $\tau_{N2O} = 109$ yr (Forster et al., 2021). Thus, their mass change dynamics due to surface flux $F_\chi(t)$ can be expressed analogously to Eq. (SI.11):

$$m_\chi(t) \approx \int_{t_{r,\chi}}^{t} F_\chi(s) e^{-(t-s)/\tau_\chi} ds\,, \quad \chi = CH_4, N_2O \qquad \text{(SI. 16)}$$

If $t - t_{r,\chi} \gg \tau_\chi$ and F_χ changes linearly with time, i.e., $F_\chi(t) = \hat{F}_{r,\chi} t + F_{r,\chi}$, $t > t_{r,\chi}$, then we can write

$$m_\chi(t) \approx \tau_\chi\left(\hat{F}_{\mathrm{r},\chi}t + F_{\mathrm{r},\chi}\right) - \tau_\chi^2\hat{F}_{\mathrm{r},\chi},\ \ \chi = \mathrm{CH_4}, \mathrm{N_2O} \qquad \text{(SI. 17)}$$

where the 'recent' period potentially affecting the current RF can be approximated as $t - t_{\mathrm{r,CH4}} = 3\tau_{\mathrm{CH4}} \approx 35$ yr and $t - t_{\mathrm{r,N2O}} = 3\tau_{\mathrm{N2O}} \approx 330$ yr. For a constant F_χ for $t > t_{\mathrm{r},\chi}$, we obtain the simple steady-state solution at $t \gg t_{\mathrm{r},\chi} + \tau_\chi$:

$$m_\chi(t) \approx \tau_\chi F_\chi,\ \ \chi = \mathrm{CH_4}, \mathrm{N_2O} \qquad \text{(SI. 18)}$$

Finally, we note that the above formulations can be applied with data on both GHG fluxes (kg s^{-1}) and flux densities (kg m^{-2} s^{-1}). The former corresponds to the full mire area, for example, in which case the lateral peatland expansion must be considered; the latter requires less information and could be applicable to a limited area or an area considered representative of the ecosystem, for example the central part of a mire complex.

References

Enting, I. G., 2007. Laplace transform analysis of the carbon cycle. Environmental Modelling & Software 22, 1488–1497, doi:10.1016/j.envsoft.2006.06.018.

Etminan, M., Myhre, G., Highwood, E. J. and Shine, K. P., 2016. Radiative forcing of carbon dioxide, methane, and nitrous oxide: A significant revision of the methane forcing. Geophysical Research Letters 43, doi:10.1002/2016GL071930.

Forster, P., Storelvmo, T., Armour, K., Collins, W., Dufresne, J.-L., Frame, D., Lunt, D.J., Mauritsen, T., Palmer, M.D., Watanabe, M., Wild, M., and Zhang, H., 2021. The Earth's Energy Budget, Climate Feedbacks, and Climate Sensitivity. In: Climate Change 2021: The Physical Science Basis. Contribution of Working Group I to the Sixth Assessment Report of the Intergovernmental Panel on Climate Change (ed. by V. Masson-Delmotte et al.), pp. 923–1054, Cambridge University Press, Cambridge, United Kingdom and New York, NY, USA, doi:10.1017/9781009157896.009.

Joos, F., Roth, R., Fuglestvedt, J. S., Peters, G. P., Enting, I. G., von Bloh, W., Brovkin, V., Burke, E. J., Eby, M., Edwards, N. R., Friedrich, T., Frölicher, T. L., Halloran, P. R., Holden, P. B., Jones, C., Kleinen, T., Mackenzie, F. T., Matsumoto, K., Meinshausen, M., Plattner, G.-K., Reisinger, A., Segschneider J., Shaffer, G., Steinacher, M., Strassman, K., Tanaka, K., Timmermann, A. and Weaver, A. J., 2013. Carbon dioxide and climate impulse response functions for the computation of greenhouse gas metrics: a multi-model analysis. Atmospheric Chemistry and Physics 13, 2793–2825, doi:10.5194/acp-13-2793-2013.

Lan, X., Tans, P. and Thoning, K. W., 2025a. Trends in globally-averaged CO2 determined from NOAA Global Monitoring Laboratory measurements. Version 2025-02, doi: 10.15138/9N0H-ZH07.

Lan, X., Thoning, K. W. and Dlugokencky, E. J., 2025b. Trends in globally-averaged CH4, N2O, and SF6 determined from NOAA Global Monitoring Laboratory measurements. Version 2025-02, doi: 10.15138/P8XG-AA10.

Meinshausen, M., Nicholls, Z. R. J., Lewis, J., Gidden, M. J., Vogel, E., Freund, M., Beyerle, U., Gessner, C., Nauels, A., Bauer, N., Canadell, J. G., Daniel, J. S., John, A., Krummel, P. B., Luderer, G., Meinshausen, N., Montzka, S. A., Rayner, P. J., Reimann, S., Smith, S. J., van den Berg, M., Velders, G. J. M., Vollmer, M. K., and Wang, R. H. J., 2020. The shared socio-economic pathway (SSP) greenhouse gas concentrations and their extensions to 2500, Geoscientific Model Development 13, 3571–3605. doi:10.5194/gmd-13-3571-2020.

Oeschger, H. and Heimann, M., 1983. Uncertainties of predictions of future atmospheric CO_2 concentrations, Journal of Geophysical Research 88, 1258–1262, doi:10.1029/JC088iC02p01258.

Trenberth, K. E. and Smith, L., 2005. The mass of the atmosphere: A constraint on global analyses. Journal of Climate 18, 864–875, doi:10.1175/JCLI-3299.1.

A practical metric for estimating the current climate forcing of natural mires

Janne Rinne[1], Juha-Pekka Tuovinen[2], Annalea Lohila[2,3]

1) Natural Resources Institute Finland, Helsinki, Finland
2) Finnish Meteorological Institute, Helsinki, Finland
3) INAR/Physics, University of Helsinki, Finland

Supplement II: Hypothetical CAR trajectories and resulting RF

Hypothetical CAR trajectories (left-hand-side panels) and the resulting radiative forcing by CO_2 (right-hand-side panels). The CAR trajectories follow the beta distribution with different shape parameters and are normalized to result in the same total accumulated carbon at time $= 0$. In the second and third set of trajectories, the CAR values after and before, respectively, the CAR maximum of the original distribution are replaced by the maximum value. Constant radiative efficiencies (Table SI.1) and perturbation time scales (Table SI.2) were assumed.

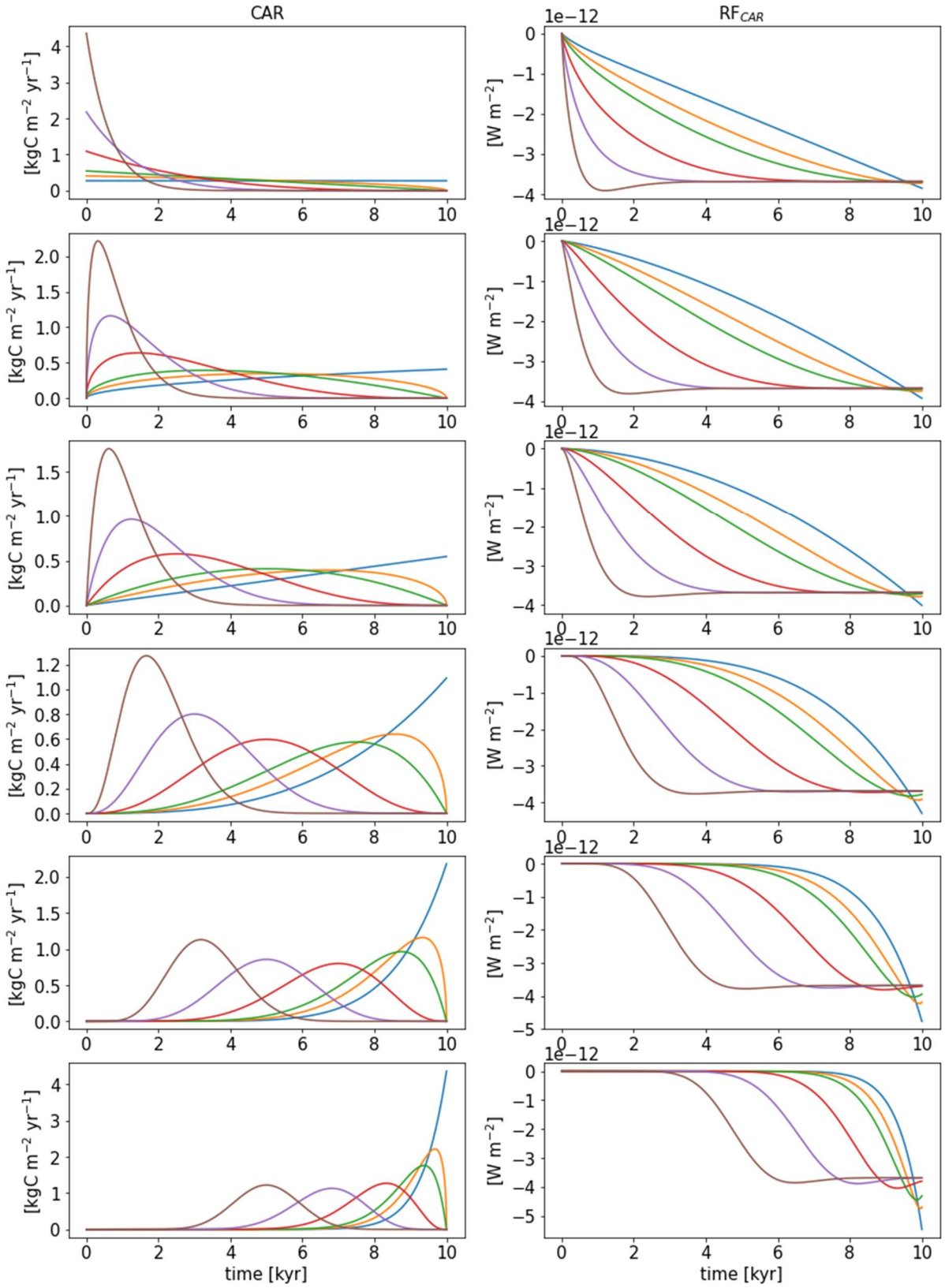
CAR
RF$_{CAR}$
[kgC m^{-2} yr^{-1}]
[W m^{-2}]
1e−12
time [kyr]
time [kyr]

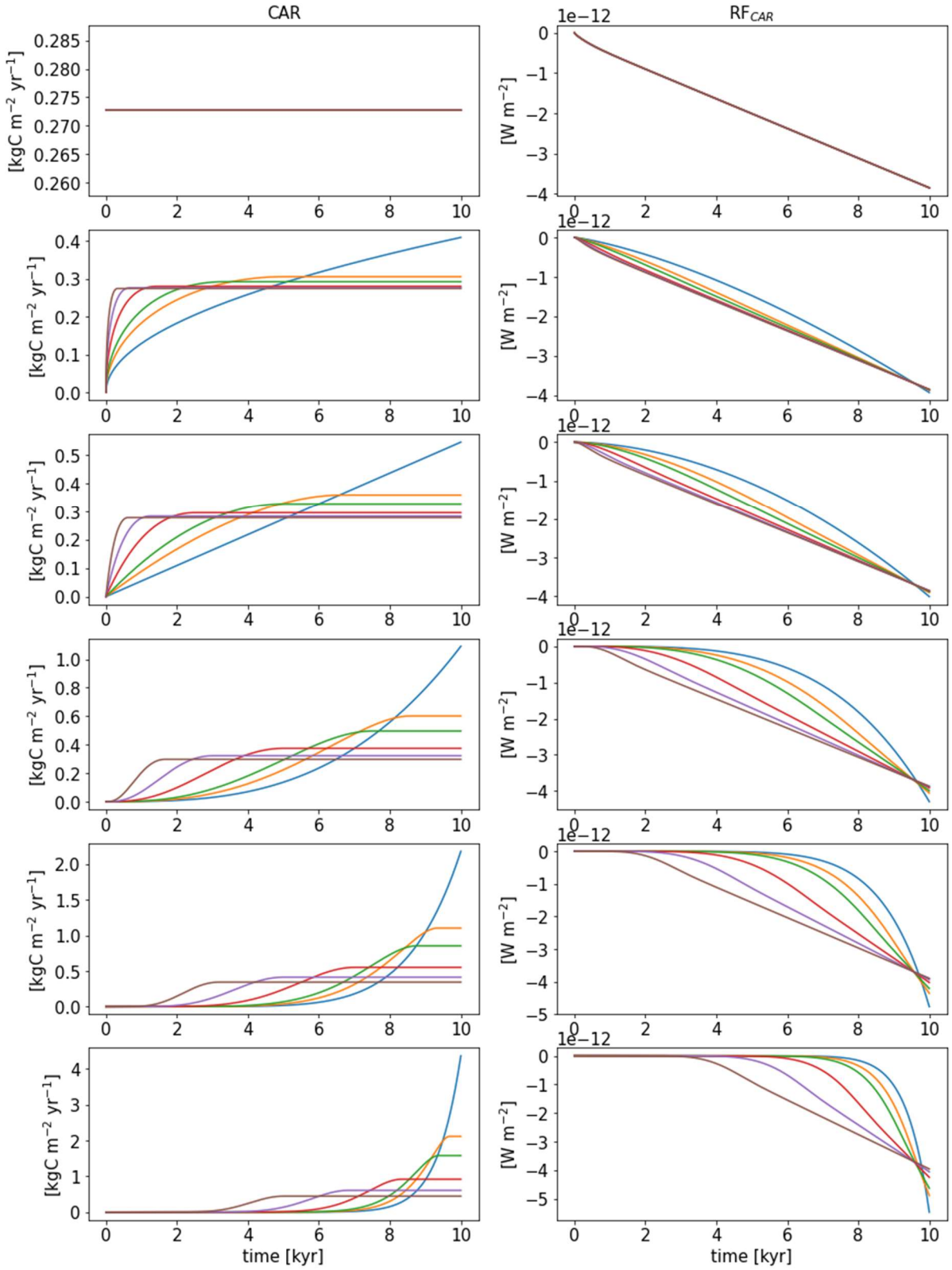
CAR
RF$_{CAR}$
[kgC m^{-2} yr^{-1}]
[W m^{-2}]
1e−12
time [kyr]
time [kyr]

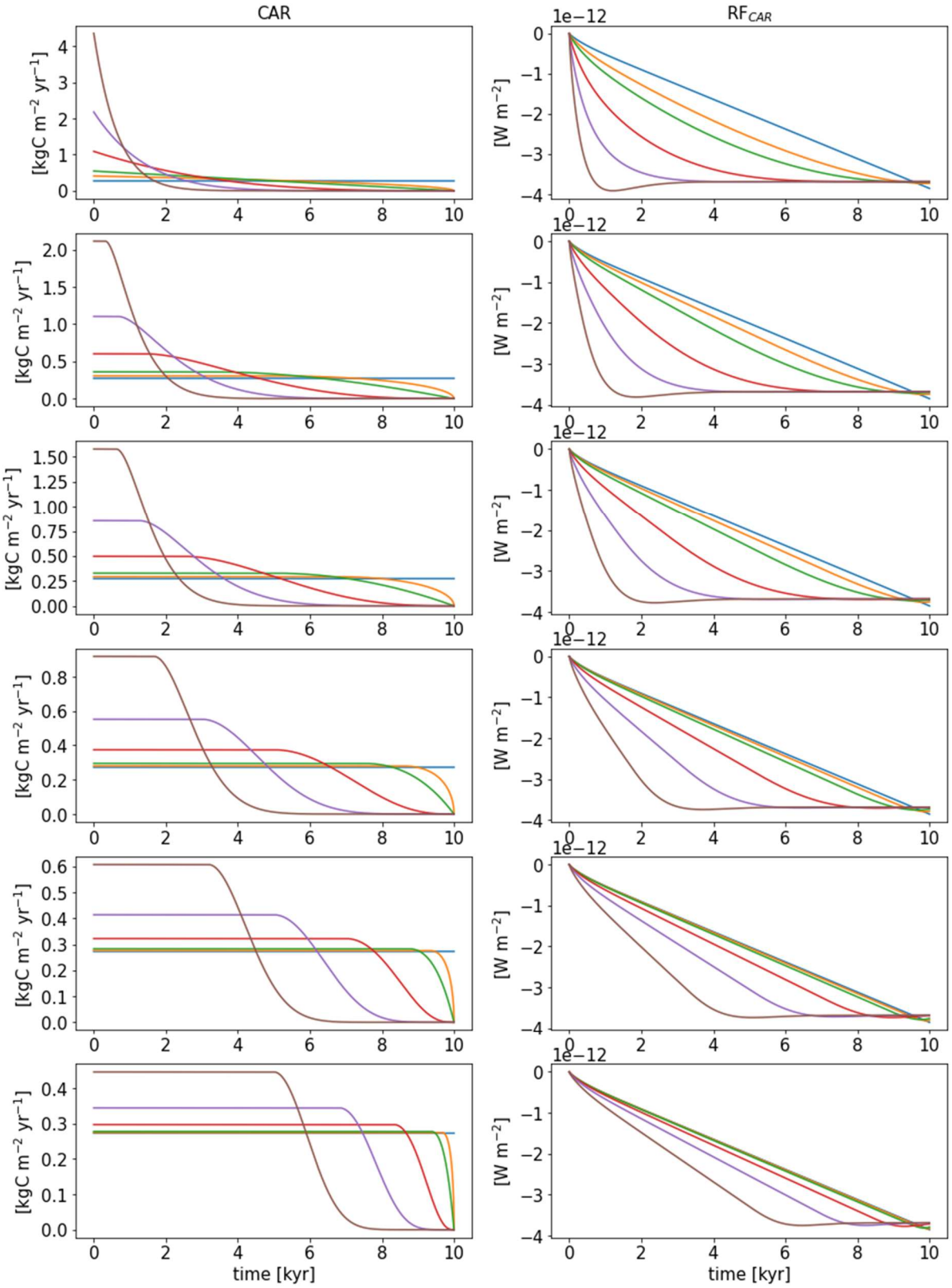
CAR
RF$_{CAR}$
[kgC m^{-2} yr^{-1}]
[W m^{-2}]
1e−12
time [kyr]

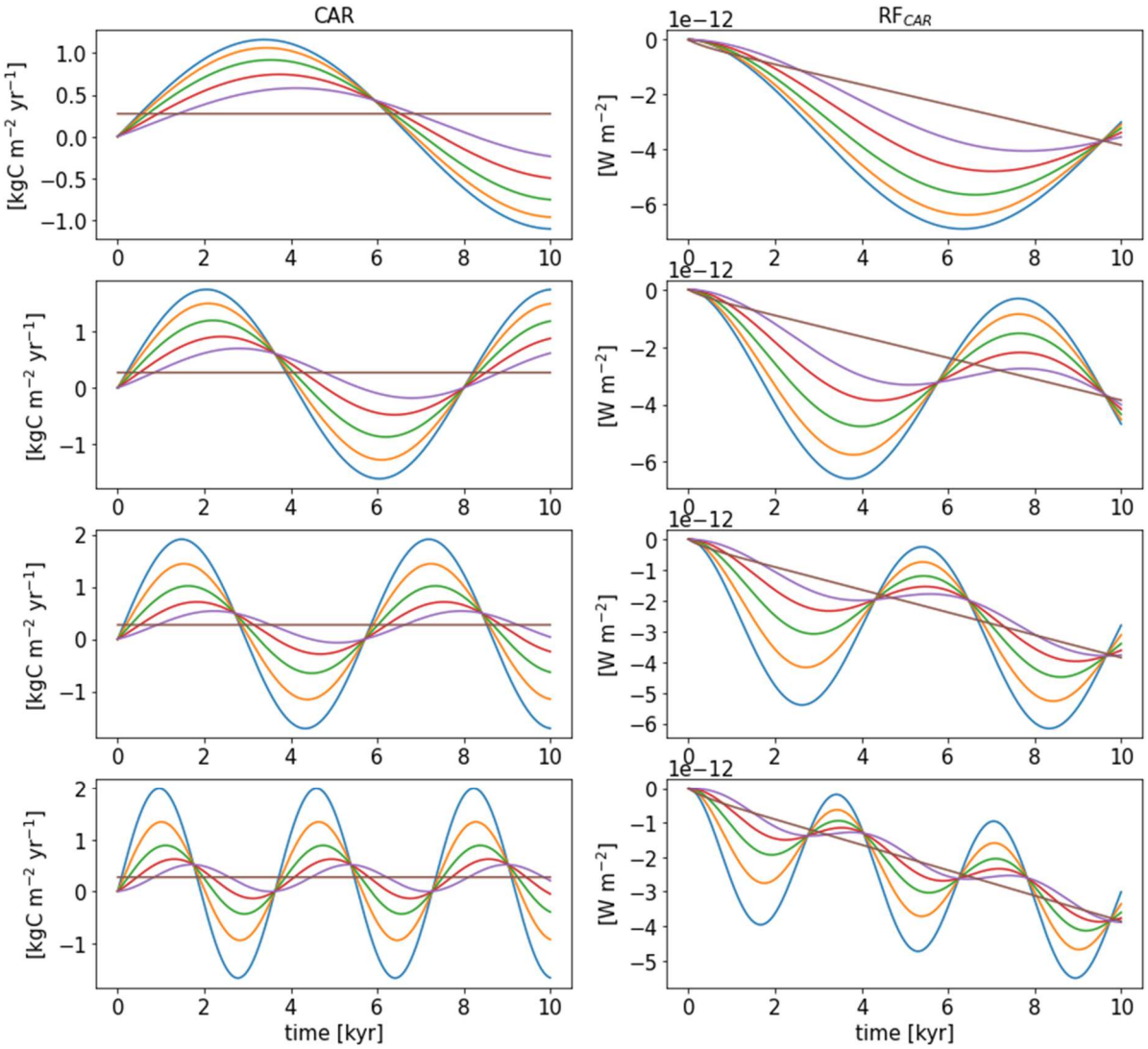
CAR
RF$_{CAR}$
[kgC m^{-2} yr^{-1}]
[W m^{-2}]
1e−12
time [kyr]
time [kyr]

A practical metric for estimating the current climate forcing of natural mires

Janne Rinne[1], Juha-Pekka Tuovinen[2], Annalea Lohila[2,3]

1) Natural Resources Institute Finland, Helsinki, Finland
2) Finnish Meteorological Institute, Helsinki, Finland
3) INAR/Physics, University of Helsinki, Finland

Supplement III: Resources for calculating the climatic effect of individual mires

SIII.1 Data for selected measurement sites for calculation of their climatic effect

The data in Table SIII.1 were collected from the cited papers, partly by digitizing their figures.

Table SIII.1. Peat core and contemporary flux data together with the calculated cumulative carbon accumulation.

Site name and location	Peat core age	Accumulated C (kg C m^{-2})	Current CH_4 flux (g CH_4 m^{-2} yr^{-1})	Current CO_2 flux (g CO_2 m^{-2} yr^{-1})	Lateral C flux (g C m^{-2} yr^{-1})	References
Lompolojänkkä (68°N, 23°E)	10000	66.1	20	-150	13*	Mathijssen et al., 2022; Aurela et al., 2015
Siikaneva (61°N, 24°E)	11500	138	13	-200	17*	Mathijssen et al., 2022; Rinne et al., 2018
Kaamanen (2 cores) (69°N, 27°E)	9385 (9270, 9500)	180	9.4	-68	4[1]	Piilo et al., 2020; Aurela et al., 2002; Juutinen et al., 2013 Heiskanen et al., 2023
Degerö (64°N, 20°E)	8282	86.7	15	-190	18[2]	Larsson et al., 2016; Nilsson et al., 2008
Mer Bleue (2 cores) (45°N, 76°W)	8000	164	4.9	-150	15[3]	Yu et al., 2002 Roulet et al., 2007

*1: Downstream loss of dissolved organic carbon (DOC), CO_2, CH_4; 2: TOC (total organic carbon) in precipitation; loss of TOC, dissolved inorganic carbon (DIC) and CH_4 through stream water runoff; 3: export of DOC. *For Lompolojänkkä and Siikaneva no data on lateral C flux is available so we assumed this to be 31% of CO_2 flux, based on average ratio of lateral C flux and CO_2 flux at the other three mires.*

SIII.2 Conversion between CO_2-eq and RF

The global warming potential of compound χ (= CH_4 or N_2O) for conversion to CO_2-equivalents was calculated according to its standard definition, i.e. as the ratio of the radiative forcing due to

a pulse emission of χ to the radiative forcing due to a corresponding CO_2 mass pulse, integrated over the selected time horizon T. For our model detailed in Supplement I, this integration yields

$$\mathrm{GWP}_{\chi}(T) = \frac{\int_0^T \varepsilon_{\mathrm{m},\chi} m_{\chi,0} e^{-t/\tau_{\chi}} dt}{\int_0^T \varepsilon_{\mathrm{m,CO2}} m_{\mathrm{CO2},0} \sum_{i=0}^{3} \alpha_i e^{-t/\tau_{\mathrm{CO2},i}}\, dt} = \frac{\varepsilon_{\mathrm{m},\chi} m_{\chi,0} \tau_{\chi}\left(1 - e^{-T/\tau_{\chi}}\right)}{\varepsilon_{\mathrm{CO2}} m_{\mathrm{CO2},0}\left[\alpha_0 T + \sum_{i=1}^{3} \alpha_i \tau_{\mathrm{CO}\ ,i}\left(1 - e^{-T/\tau_{\mathrm{CO2},i}}\right)\right]} \quad \text{(SIII. 1)}$$

where $\varepsilon_{\mathrm{m},\chi}$ and $\varepsilon_{\mathrm{m,CO2}}$ are the radiative efficiencies of χ and CO_2, respectively, $m_{\chi,0}$ and $m_{\mathrm{CO2},0}$ are the mass pulses to the atmosphere at time $t = 0$, τ_{χ} and $\tau_{\mathrm{CO2},i}$ are atmospheric perturbation time scales, and the coefficients α_i are the fractions of CO_2 allocation to the conceptual reservoirs of the model. By dividing both the numerator and denominator of the right-hand side of Eq. (SIII.1) by T and setting $m_{\chi,0} = F_{\chi} T$ and $m_{\mathrm{CO2},0} = F_{\mathrm{CO2}} T$, where F_{χ} and F_{CO2} are the current fluxes of χ and CO_2, respectively, we can define the average radiative forcing of χ and CO_2 corresponding to Eq. (SIII.1) as

$$\overline{RF}_{\chi}(T) = \varepsilon_{\mathrm{m},\chi} F_{\chi} \tau_{\chi}\left(1 - e^{-T/\tau_{\chi}}\right) \quad \text{(SIII. 2)}$$

and

$$\overline{RF}_{\mathrm{CO2}}(T) = \varepsilon_{\mathrm{m,CO2}} F_{\mathrm{CO2}} \left[\alpha_0 T + \sum_{i=1}^{3} \alpha_i \tau_{\mathrm{CO}\ ,i}\left(1 - e^{-T/\tau_{\mathrm{CO2},i}}\right)\right] \quad \text{(SIII. 3)}$$

In Figure 2 the CH_4 emission was converted to CO_2 equivalents by multiplying the mass flux of CH_4 by $\mathrm{GWP}_{\mathrm{CH4}}(100\ \mathrm{yr}) = 24.9$, and the corresponding radiative forcing components were calculated using Eqs. (SIII.2) and (SIII.3) and the parameter values presented in Supplement I.

SIII.3 Data for full impulse-response model

The CAR data from Mer Bleue for the calculation with the full impulse-response model were digitized from Roulet et al. (2007). For the past 1000 years, the data were digitized by the highest possible time resolution (typically 10-50 years). For the time before this we used a 1000-year resolution. All data were then linearly interpolated to annual values. A constant CH_4 emission, obtained from recent measurements (Table SIII.1), was used as further input to the explicit RF model.

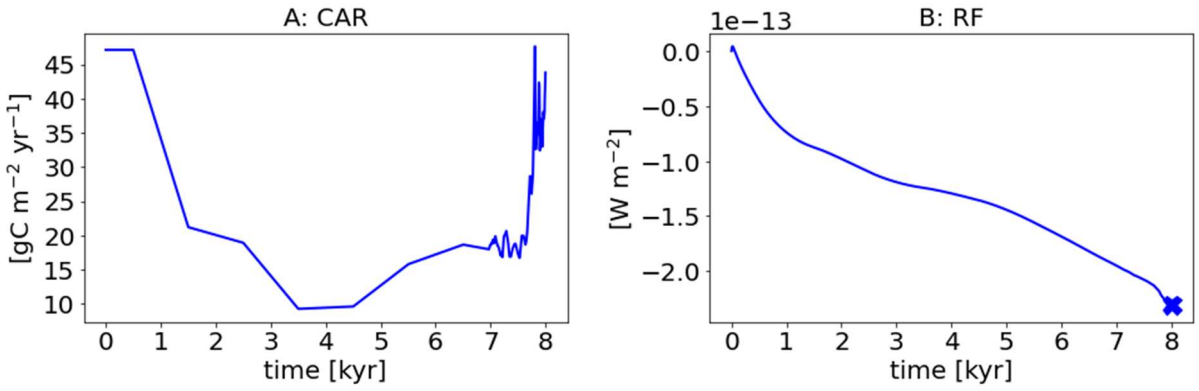

Figure SIII.1. CAR time series from Mer Bleue (A) and the resulting RF calculated with the full impulse-response model (B). Constant methane emission (Table SIII.1) was assumed in the calculation. The cross indicates the RF estimated with the ACME coefficients. Constant radiative efficiencies (Table SI.1) and perturbation time scales (Table SI.2) were assumed.

References

Aurela M, Laurila T and Tuovinen J-P 2002 Annual CO2 balance of a subarctic fen in northern Europe: Importance of the wintertime efflux. *Journal of Geophysical Research* **107** 4607

Aurela M, Lohila A, Tuovinen J-P, Hatakka J, Penttilä T and Laurila T 2015 Carbon dioxide and energy flux measurements in four northern-boreal ecosystems at Pallas. *Boreal Environmental Research* **20** 455-473

Heiskanen L, Tuovinen J-P, Vekuri V, Räsänen A, Virtanen T, Juutinen S, Lohila A, Mikola J and Aurela M 2023 Meteorological responses of carbon dioxide and methane fluxes in the terrestrial and aquatic ecosystems of a subarctic landscape. *Biogeosciences* **20** 545–572

Juutinen S, Väliranta M, Kuutti V, Laine A M, Virtanen T, Seppä H, Weckström J and Tuittila E-S 2013 Short-term and long-term carbon dynamics in a northernpeatland-stream-lake continuum: A catchment approach *J Geophys Res: Biogeosciences* **118** 171–183

Larsson A, Segerström U, Laudon H and Nilsson M B 2017 Holocene carbon and nitrogen accumulation rates in a boreal oligotrophic fen. *The Holocene* **27** 811-821 (doi: 10.1177/0959683616675936)

Mathijssen P J H., Tuovinen JP, Lohila A, Väliranta M and Tuittila ES 2022 Identifying main uncertainties in estimating past and present radiative forcing of peatlands. *Global Change Biology* **28** 4069-4084.

Nilsson M, Sagerfors J, Buffam I, Laudon H, Eriksson T, Grelle A, Klemedtsson L, Weslien P and Lindroth A 2008 Contemporary carbon accumulation in a boreal oligotrophic minerogenic mire – a significant sink after accounting for all C-fluxes. Global Change Biology, 14: 2317-2332.

Piilo S et al 2020 Spatially varying peatland initiation, Holocene development, carbon accumulation patterns and radiative forcing within a subarctic fen. *Quaternary Science Reviews* **248** 106596 (doi: 10.1016/j.quascirev.2020.106596

Rinne J *et al* 2018 Temporal variation of ecosystem scale methane emission from a boreal fen in relation to temperature, water table position, and carbon dioxide fluxes. *Global Biogeochemical Cycles* **32**, 1087-1106

Roulet N T, Lafleur P M, Richard P J H, Moore T R, Humphreys E R and Bubier J 2007 Contemporary carbon balance and late Holocene carbon accumulation in a northern peatland. *Global Change Biology* **13** 397-411 (doi: 10.1111/j.1365-2486.2006.01292.x)

Yu Z C, Bhatti J S, Apps M J technical coordinators 2002 Long Term Dynamics and Contemporary Carbon Budget of Northern Peatlands. Proc. International Workshop on Carbon Dynamics of Forested Peatlands: Knowledge Gaps, Uncertainty, and Modeling Approaches, 23-24 March 2001,

Edmonton, AB. Nat. Resour. Can., Can. For. Serv., North. For. Cent., Edmonton, AB. Inf. Rep. NOR-X-383. https://ostrnrcan-dostrncan.canada.ca/entities/publication/9ea11a43-bdd1-46dd-9688-174d32c1d2b9